NANO LETTERS
Letter
Cite This: Nano Lett. 2019, 19, 7673−7680
pubs.acs.org/NanoLett

Optically Driven Magnetic Phase Transition of Monolayer $RuCl_3$

Yingzhen Tian,[†,⊥] Weiwei Gao,[‡,⊥] Erik A. Henriksen,[†] James R. Chelikowsky,[*,‡,§,∥] and Li Yang[*,†]

[†]Department of Physics and Institute of Materials Science and Engineering, Washington University, St. Louis, Missouri 63130, United States

[‡]Center for Computational Materials, Oden Institute for Computational Engineering and Sciences, [§]Department of Physics, and [∥]McKetta Department of Chemical Engineering, The University of Texas at Austin, Austin, Texas 78712 United States

Supporting Information

ABSTRACT: Strong light-matter interactions within nanoscale structures offer the possibility of optically controlling material properties. Motivated by the recent discovery of intrinsic long-range magnetic order in two-dimensional materials, which allow for the creation of novel magnetic devices of unprecedented small size, we predict that light can couple with magnetism and efficiently tune magnetic orders of monolayer ruthenium trichloride ($RuCl_3$). First-principles calculations show that both free carriers and optically excited electron−hole pairs can switch monolayer $RuCl_3$ from a proximate spin-liquid phase to a stable ferromagnetic phase. Specifically, a moderate electron−hole pair density (on the order of 1×10^{13} cm^{-2}) can significantly stabilize the ferromagnetic phase by 10 meV/f.u. in comparison to the competing zigzag phase, so that the predicted ferromagnetism can be driven by optical pumping experiments. Analysis shows that this magnetic phase transition is driven by a combined effect of doping-induced lattice strain and itinerant ferromagnetism. According to Ising-model calculations, we find that the Curie temperature of the ferromagnetic phase can be increased significantly by raising carrier or electron−hole pair density. This enhanced optomagnetic effect opens new opportunities to manipulate two-dimensional magnetism through noncontact, optical approaches.

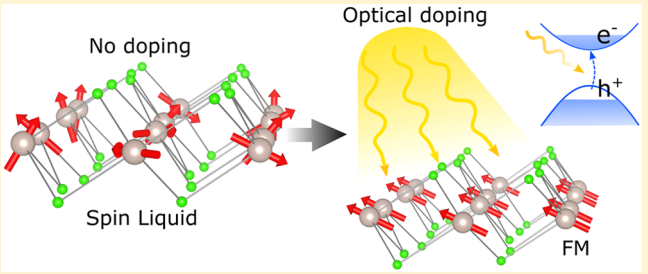

KEYWORDS: *2D ferromagnetism, $RuCl_3$, optomagnetic effects, first-principles method, electrostatic doping*

Since the discovery of graphene, new classes of atomically thin materials, such as transition metal dichalcogenides (TMDs), black phosphorus, and many others, have been synthesized. Such materials display a wide range of remarkable mechanical, optical, and electronic properties, which only appear in their two-dimensional (2D) forms. Particular efforts have been invested in realizing ferromagnetism in 2D materials, such as applying an external strain,[1,2] doping,[3] introducing adatoms,[4] or using proximity effects.[5] Recently, intrinsic ferromagnetism that persists in the 2D limit was observed in monolayer CrI_3,[6] monolayer and few-layer $CrXTe_3$ (X = Ge, Si),[7,8] VSe_2,[9] Fe_3GeTe_2,[10] and so forth.[11,12] These materials offer new opportunities for studying spin physics in low dimensions, and for designing spintronic devices of unprecedentedly small size.[12,13] Following these seminal discoveries, several groups independently demonstrated the tunability of magnetic orders of 2D systems.[14,15] For example, they found that the interlayer coupling of bilayer CrI_3 can be reversibly tuned from the antiferromagnetic (AFM) to the ferromagnetic (FM) phase by changing the free-carrier concentration via gate voltage.[14,15]

Beyond mechanical strain, chemical doping, and electrostatic gating, optically tuning material properties are highly preferable as no contacts are involved. The enhanced light-matter interactions in layered van der Waals (vdW) materials strengthen the possibility to optically control material properties.[16,17] Laser induced structural phase transitions in TMDs,[18] photoinduced insulator-to-metal phase transition in VO_2 thin film,[19−21] optically tunable magnetism,[22−24] and light-induced superconductivity in cuprates[25] are examples of light-controlled properties in materials. Enhanced opto-piezoelectric effects have been predicted in monolayer group IV−VI materials as well.[26] The recent breakthrough in 2D magnetism suggests a search for optically tunable magnetism in 2D systems.

Among magnetic vdW materials, α-$RuCl_3$ is a good candidate to search for opto-magnetic effects. Similar to $CrXTe_3$ (X = Ge, Si) and CrI_3, α-$RuCl_3$ is a layered material with weak vdW interactions between layers. First-principles calculations show that α-$RuCl_3$ has a small cleavage energy, and monolayer (and few-layer) $RuCl_3$ has recently been obtained through mechanical exfoliation in experiment.[27−29] Bulk α-$RuCl_3$ displays an in-plane "zigzag" antiferromagnetic (zigzag AFM) order[30] where the magnetic moments of Ru^{3+} ions align ferromagnetically with other Ru^{3+} in the same zigzag chain and antiferromagnetically with those in neighboring zigzag chains. Recent studies have shown that α-$RuCl_3$ is a

Received: June 21, 2019
Revised: October 2, 2019
Published: October 22, 2019

DOI: 10.1021/acs.nanolett.9b02523
Nano Lett. 2019, 19, 7673−7680

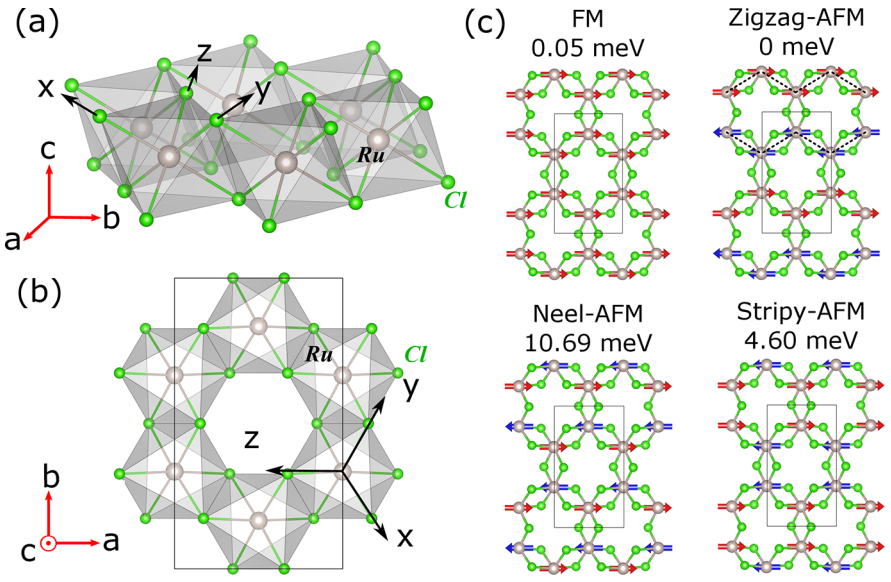

Figure 1. (a,b) Top and side views of the crystal structure of monolayer $RuCl_3$ (plot with VESTA[36]). The rectangle shows the 16-atom supercell used in our calculations. (c) Schematic plots of the supercell and spin configurations of four magnetic orders, that is, the ferromagnetic, zigzag AFM, Neel-AFM, and stripy AFM phases. The zigzag chains in zigzag-AFM phase are shown as dashed lines. The relative energies (per formula unit) to the zigzag AFM state are presented as well.

possible system for studying the Kitaev model. This model is exactly solvable and hosts rich and exotic magnetic phenomena, including bond-dependent exchange coupling, rich quantum spin liquid phases and fractional excitations.[31] These interesting magnetic properties can possibly be retained in the monolayer limit, given that the interlayer exchange coupling is only a few percent of the intralayer exchange coupling according to ab initio calculations,[32] and the anisotropic alignment of magnetic moments of Ru ions provides the necessary condition for long-range 2D magnetic order, according to the Mermin−Wagner theorem.[7,33]

Here, we show that unipolar doping and optical electron-hole (e-h) bipolar doping can be efficient approaches to switch the ground state of monolayer $RuCl_3$ from the proximate spin-liquid phase to the FM order. The critical carrier densities for realizing this magnetic phase transition are moderate, that is, on the order of 10^{13} cm^{-2} for electrons, holes, and photoexcited e-h pairs. As a result, 2D ferromagnetism can be turned on/off by electrostatic gating and, more interestingly, by optical pumping with a practical e-h density. Moreover, we find that the electron-doping-driven FM order is mainly from lattice distortions, whereas the hole- and e-h pair-driven FM orders are mainly from itinerant electrons. The estimated Curie temperature based on an Ising model is above the liquid-nitrogen temperature and can be further increased by higher carrier/e-h pair densities.

Results and Discussion. *Structural and Magnetic Properties.* Monolayer $RuCl_3$ has a structure similar to the monolayer ferromagnetic CrI_3. As shown in Figure 1a,b, Ru^{3+} ions bond with the six nearest-neighbor Cl^{1-} ions, forming edge-sharing $RuCl_6$ octahedra, which show trigonal distortions from the regular octahedron.[27,30] The zigzag AFM spin configuration enlarges the hexagonal unit cell to be an orthorhombic supercell containing 16 atoms, as shown in Figure 1b. This supercell is used for our calculations and discussions unless otherwise stated.

Depending on the ratio of the Heisenberg exchange and Kitaev interaction, the solution of the Heisenberg−Kitaev model[34] corresponds to four phases with long-range magnetic orders: the zigzag, Neel, Stripy, and ferromagnetic phases in intrinsic monolayer $RuCl_3$. To elucidate the spin configurations of these phases, we schematically plot the arrangement of the local magnetic moments of Ru^{3+} ions with colored arrows in Figure 1c. Using an effective Hubbard $U_{eff} = U - J$ of 2 eV,[32,35] our ab initio density functional theory (DFT) calculations reveal that the zigzag AFM phase has the lowest energy among four magnetic phases. The competing FM phase has a slightly higher energy of ∼0.05 meV per formula unit (f.u.) relative to the zigzag phase. The energies of the Neel and stripy AFM phases are notably higher (more than 4.6 meV/f.u.) than the other two. These relative energies are summarized in Figure 1c and agree well with a previous work.[35] By checking the effects of Hubbard U_{eff} value on our calculations, we find the energy ordering of four magnetic phases (i.e., E(Zigzag) ≈ E(FM) < E(stripy) < E(Neel)) remain the same for the range of U_{eff} from 2 to 5 eV (see Figure S1 in Supporting Information).

Although our calculation shows that the zigzag AFM phase has the lowest energy among four spin configurations, the small energy difference between the zigzag AFM and FM phases is only 0.05 meV/f.u. within the accuracy of the DFT +U approach. This indicates that the zigzag AFM phase and FM phase are nearly degenerate in the undoped situation. Debates on the magnetic order of monolayer $RuCl_3$ also exists in the literature. For example, Iyikanat et al. predicted that the zigzag AFM phase is the ground state,[35] whereas Sarikurt et al. predicted that the competing FM phase is the ground state.[37] Nevertheless, both works show the energy difference between the zigzag AFM and FM phases is small (less than 1.2 meV/f.u.). The discrepancy between different calculations is due to the enhanced magnetic frustration in single-layer $RuCl_3$, as shown in a recent Raman scattering experiment.[29] In particular, as the dimension of $RuCl_3$ changes from bulk to monolayer, the experiment[29] shows the increasingly strong phonon-magnetic scattering, a hallmark of quantum spin liquids. These experimental and theoretical evidence support

DOI: 10.1021/acs.nanolett.9b02523
Nano Lett. 2019, 19, 7673−7680

that the undoped monolayer $RuCl_3$ is in a proximate quantum spin-liquid phase.

Effects of Unipolar Doping. We consider the role of unipolar doping on the magnetic order of monolayer $RuCl_3$. The doped free carriers are introduced by the electrostatic doping approach, which has been widely applied to studying free-carrier doping effects on magnetism[38−40] and realized by voltage gating approaches in experiment.[10,14] In Figure 2a, we

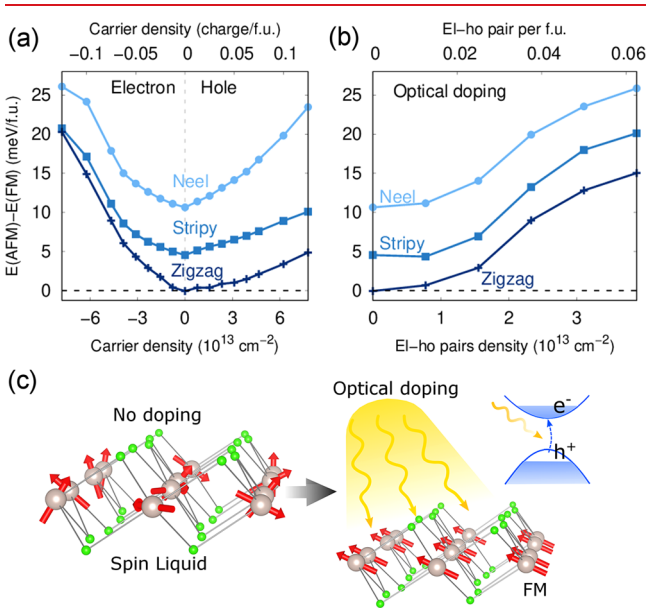

Figure 2. (a,b) The relative energies to the zigzag AFM phase of monolayer $RuCl_3$ for unipolar doping and optical e-h doping, respectively. (c) Schematic plot of the optically tunable 2D magnetism in $RuCl_3$.

present the total energies of three AFM phases (i.e., zigzag, Neel, and stripy phases) relative to that of the FM phase (denoted as $E(\mathrm{AFM}) - E(\mathrm{FM})$) under different doping densities. The Neel and stripy AFM phases always have significantly higher energies within a reasonable range of doping densities. Therefore, we focus on the competition between the FM and zigzag AFM phases.

As shown in Figure 2a, $E(\mathrm{Zigzag}) - E(\mathrm{FM})$ changes from a small negative value to positive as the concentration of free carriers (either electrons or holes) increases. This suggests that doped monolayer $RuCl_3$ energetically prefers the FM phase over the zigzag AFM phase. For example, to induce an $E(\mathrm{Zigzag}) - E(\mathrm{FM}) > 5$ meV/f.u., one needs to dope around 4×10^{13} cm^{-2} electrons or 8×10^{13} cm^{-2} holes. Such carrier densities are comparable with the critical density (2.6×10^{13} cm^{-2}) for the doping-induced magnetic phase transition of bilayer CrI_3.[14,15] In particular, the energy difference between the zigzag AFM and FM phases can be increased to around 20 meV/f.u. with an electron doping density of 7.7×10^{13} cm^{-2}. For reference, a recently experimentally confirmed room-temperature 2D magnet VSe_2[9] displays an energy difference of 24 meV/f.u. between the FM and AFM orders by first-principles calculations.[1] Accordingly, we expect that unipolar doping can drive the ground state from the nearly degenerate magnetic orders to the FM order. Finally, we have checked the doping and screening impacts on the effective onsite Coulomb interaction U_{eff}. Using the linear-response method,[41] we calculated that the variation of U_{eff} between doping densities of 0.20 electron/supercell and 0.20 hole/supercell is about 0.2 eV. Therefore, this small variation of U_{eff} will not change the above conclusion.

Effects of Optical Doping. An important characteristic of $RuCl_3$ is that unlike bilayer CrI_3[14] and monolayer GaSe[38] in which only one type of free carrier can tune the magnetic order, monolayer $RuCl_3$ transits to the FM phase by either electron doping or hole doping. This indicates a possible optical doping effect[42−44] in which photoexcited electrons and holes are created simultaneously to drive the magnetic phase transition. To study the role of photoexcited electrons and holes, we employ a constrained DFT approximation, in which we manually change the occupation numbers of valence and conduction states to mimic the simultaneous existence of photoexcited electrons and holes. This approach has successfully been applied to examine excited-state structures of defects[45,46] and photoinduced structural changes (perovskites and monolayer SnSe).[26,47] The effects of optical doping are modeled with 64-atom supercells.

Figure 2b illustrates the total energies of three AFM phases relative to the FM phase (denoted as $E(\mathrm{AFM}) - E(\mathrm{FM})$) as a function of optical doping. Focusing on the competition between the FM and zigzag AFM phases, $E(\mathrm{Zigzag}) - E(\mathrm{FM})$ increases monotonically with the density of e-h pairs. A significant energy difference between the FM and zigzag AFM phases of approximately 12 meV/f.u. is observed under a moderate e-h pair density of 3.0×10^{13} cm^{-2}. This suggests the possibility to tune magnetic properties of 2D $RuCl_3$ by noncontacting optical approaches. We plot such a photo-induced magnetic effect schematically in Figure 2c.

Next, we discuss the feasibility of observing photoinduced magnetic phase transition in experiments. In monolayer transition metal dichalcogenide,[44,48] optical pumping can generate e-h pairs with densities up to 10^{14} cm^{-2}, which could be large enough to stabilize the FM phase. The photoinduced ferromagnetism can then be detected with the time-resolved magneto-optical Kerr effect, which measures magnetic responses in the time scale of a femtosecond.[49,50] Another way to observe the photoinduced ferromagnetism in monolayer $RuCl_3$ is to apply continuous light illumination, which can ensure the photoexcited carriers to reach equilibrium. This approach has been demonstrated experimentally. By using light-emitting diode, Náfrádi et al. demonstrate the melting of ferromagnetism in $CH_3NH_3(Mn:Pb)I_3$ due to the photoinduced carriers.[22]

Finally, the imbalance of electron and hole concentration caused by extrinsic factors, such as deep-level defects,[48] are not considered in our calculations. However, as seen in Figure 2a, unipolar doping also strongly favors the FM order, making our prediction robust to different concentrations of electrons and holes.

The Mechanism of the Doping and Optomagnetic Effects. It is important to understand the mechanism of the doping-induced effect on magnetic order. First, we realize that the structural variation induced by doping could be an important factor to favor the FM order. Doped carriers can substantially change the lattice constants of monolayer $RuCl_3$, and strain is also known to impact the magnetic order.[32,35] Within the range of ±0.075 electron/f.u. doping density, as shown in Figure 3a, the in-plane lattice constants, a and b, monotonically vary within 2%. When the type of free carriers changes from hole to electron, the in-plane strain changes from compressive to tensile. Interestingly, as shown in Figure 3b, if

DOI: 10.1021/acs.nanolett.9b02523
Nano Lett. 2019, 19, 7673−7680

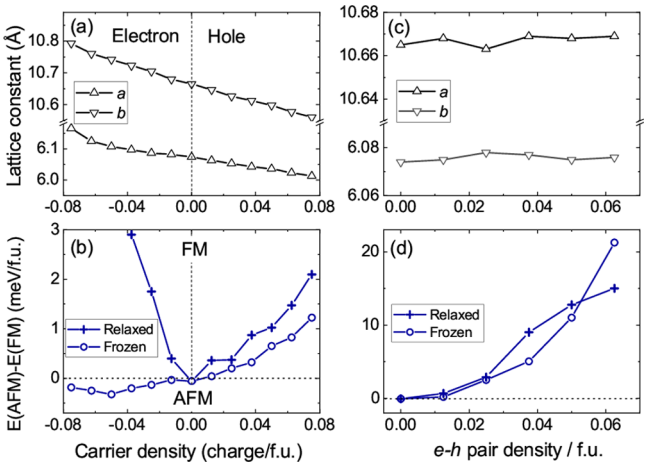

Figure 3. (a,c) The lattice constants of the supercell of monolayer $RuCl_3$ according to the unipolar and optical dopings, respectively. (b,d) The energy difference between the FM and zigzag AFM phases according to the unipolar and optical dopings, respectively. Results calculated with fully relaxed and frozen structures under doping are compared. Note the data points for relaxed structures (plotted with small cross) in (b,d) are the same as Figure 2a,b, respectively.

we fix the crystal structure as that of the undoped situation, electron doping does not favor the FM order. Therefore, electron doping induces a tensile strain that is crucial to favoring the FM order. On the other hand, the hole doping shrinks the in-plane lattice constants (Figure 3a) and, moreover, e-h optical doping does not change the lattice constants significantly, as shown in Figure 3c. Even if we fix the crystal structure, hole doping and e-h optical doping still change the relative energies between the FM and zigzag AFM orderings, as shown in Figure 3b,d, indicating that they have a different mechanism to choose the FM order.

Many factors influence the magnetic order of solids. For doped monolayer $RuCl_3$, we identify that both itinerant electrons and localized magnetic moments contribute significantly to the doping induced ferromagnetism.

For the first mechanism, that is, the itinerant magnetism, we calculated the density of state (DOS) for monolayer intrinsic $RuCl_3$ in a nonmagnetic state. Van Hove singularities (vHSs) in the DOS appear right above and below the Fermi energy, as shown in Figure 4a, and the vHS below the Fermi energy has a particularly higher peak than the vHS above the Fermi energy.

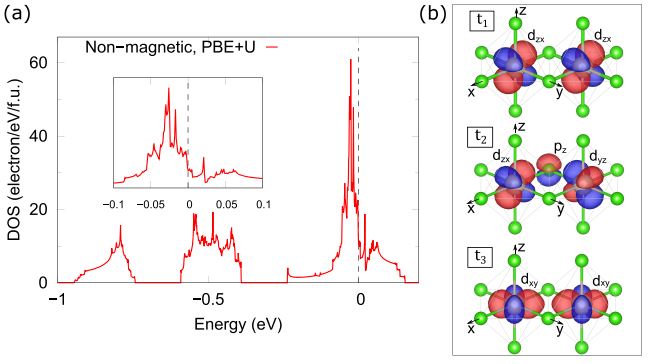

Figure 4. (a) DOS of intrinsic monolayer $RuCl_3$ in a nonmagnetic state. This plot is calculated with the structure relaxed with the Zigzag AFM phase. Inset: the zoom-in plot of DOS near the Fermi energy. (b) Schematic plots of the hopping channels between t_{2g} orbitals.

These vHSs have the characteristics of localized Ru t_{2g} orbitals. According to the Stoner's theorem, if the structure is frozen as the intrinsic (undoped) case, hole doping and optical doping that also introduces holes shift the Fermi energy to vHSs with higher DOS and are more likely to induce the Stoner's instability than electron doping. This qualitatively explains why hole doping and optical doping favors the FM order even if we froze the structure at the intrinsic situation.

In addition to itinerant magnetism, the direct and indirect exchange couplings between localized moments of Ru^{3+} also affect the magnetic order of doped monolayer $RuCl_3$. This is particularly important for the case of electron doping. Rau et al.[34] proposed a generic spin model to study magnetic phase diagrams for materials with honeycomb-layered structures similar to the A_2IrO_3 (A = Na, Li) family iridates and $RuCl_3$. We will employ this analytical model to analyze the couplings between localized magnetic moments in carrier or optically doped monolayer $RuCl_3$. This spin model considers the Heisenberg interaction (J), Kitaev interaction (K), and symmetric off-diagonal exchange interaction (Γ) for the honeycomb lattice.

These magnetic interactions (J, K, and Γ) are determined by three hopping integrals, denoted as t_1, t_2, and t_3, between Ru t_{2g} orbitals, which are schematically plotted in Figure 4b. We construct the tight-binding Hamiltonian using maximally localized Wannier functions[51] for the t_{2g} orbitals of Ru atoms and obtain the hopping integrals t_i (i = 1, 2, 3) from the tight-binding Hamiltonian. Then, we calculate the exchange parameters J, K, and Γ for a few different doping conditions, as shown in Table 1. Details on calculating hopping integrals and exchange parameters are presented in the Supporting Information.

Table 1. Exchange Coupling Constants Calculated from Tight-Binding Hopping Parameters

doping density (f.u.$^{-1}$)	J (meV)	K	Γ	ϕ	Θ
−0.075 (electron)	−4.69	9.47	−0.91	0.646π	0.527π
0.0	−5.31	11.46	−1.42	0.638π	0.536π
0.075 (hole)	−6.10	13.55	−1.92	0.635π	0.541π

Overall, we find that the Heisenberg exchange J is ferromagnetic, whereas the Kitaev exchange K is antiferromagnetic. The magnitude of Kitaeve interaction K is about twice the Heisenberg interaction J. The off-diagonal term Γ is ferromagnetic and smaller than K by an order of magnitude. According to the phase diagram of the generic spin model,[34] the magnetic order of $RuCl_3$ is determined by the $\phi = \arctan\left(\frac{J}{K}\right)$ and $\theta = \arctan\left(\frac{\sqrt{J^2+K^2}}{\Gamma}\right)$, that is, the ratio between J, K, and Γ. The intrinsic $RuCl_3$ has a zigzag AFM phase. As doping carriers change from holes to electrons, the parameter ϕ increases monotonically from 0.635π (hole doping) to 0.646π (electron doping), during which the structure is relaxed and thus the corresponding strain effect is included. This drives the system toward the FM phase. This qualitatively explains that electron-doping induces ferromagnetism through strain effects and variation of exchange couplings. On the other hand, we note that although the changing trend of ϕ qualitatively prefers the FM order, the variation value is smaller than the threshold value in ref 34. One reason can be that it is hard to get close quantitative

DOI: 10.1021/acs.nanolett.9b02523
Nano Lett. 2019, 19, 7673−7680

agreements between models and first-principles calculations in correlated magnetic materials. Meanwhile, the electron-induced FM order benefits from both exchange interactions and itinerant magnetism.

Estimation of Curie Temperature. To estimate the Curie temperature of the doping-induced FM phase, we fit the total energies of these four spin configurations with a 2D Ising model, including up to the third nearest-neighbor (NN) exchange coupling, and extract the exchange coupling constants. In Figure 5a,b, we present the calculated exchange

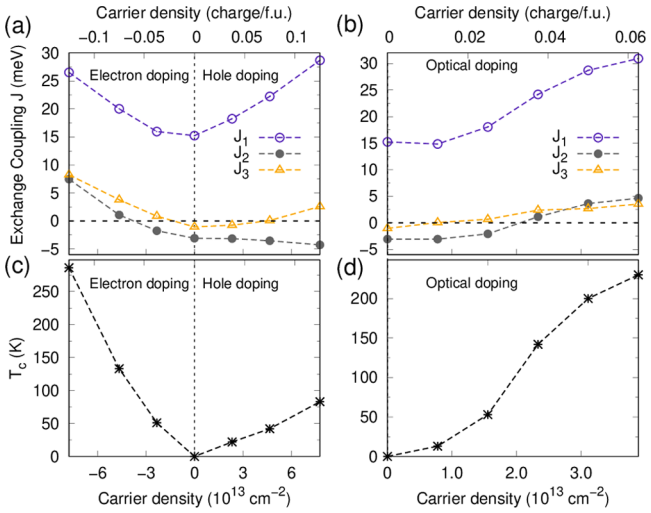

Figure 5. (a,b) The exchange coupling constants (J_1, J_2, and J_3) according to the unipolar doping and optical e-h doping, respectively. (c,d) The MC simulated Curie temperature of monolayer $RuCl_3$ under the unipolar doping and optical e-h doping, respectively.

coupling constants under different doping densities. Under electron doping, the magnitude of the second NN exchange coupling J_2 and the third NN exchange coupling J_3 can be as large as 8 meV, which is comparable to the NN coupling J_1. Interestingly, J_1 remains to be positive (i.e., supporting the FM order) under different doping conditions and increases with the carrier concentration. Previous experimental work[52] also supports that the coupling between NN Ru is FM.

With the exchange coupling constants J_i (i = 1, 2, 3) as inputs, we estimate the Curie temperature T_c of the doping-induced FM phases using Monte Carlo (MC) simulations based on the Metropolis algorithm. Figure 5c,d shows T_c for different doping densities. The estimated T_c can be significantly increased under doping with the provision that the Ising model is a rough estimation, which tends to overestimate the Curie temperature.

In summary, we performed first-principles calculations to investigate the ground-state of monolayer $RuCl_3$ under electrostatic and optical dopings. Our calculations show that an intrinsic monolayer $RuCl_3$ has nearly degenerate FM and zigzag AFM ordering. These results and previous work both indicate that the undoped monolayer $RuCl_3$ shows signatures of strong magnetic frustrations and quantum spin liquid. We predict that electrostatic doping with either electrons or holes and optical doping can both cause a phase transition from the spin-liquid phase to the FM order with a moderate carrier/e-h density, achievable with current experimental techniques. Increasing e-h pair density by optical doping can further enhance ferromagnetism and increases the Curie temperature significantly. The mechanisms for driving the magnetic phase transition are discussed based on itinerant magnetism and an analytical model of orbital magnetism. In brief, electron doping drives the magnetic phase transition mainly by inducing a tensile strain that changes the exchange coupling between Ru 4d orbitals, whereas hole doping and optical electron−hole doping enhances ferromagnetism through itinerant electrons. Optically driving 2D ferromagnetism offers the possibility of noncontact tunability for exploring new physics and spintronic applications.

Computational Details. We carry out pseudopotential DFT calculations with the plane-wave based Quantum Espresso code.[53,54] The Perdew−Burke−Ernzerhof (PBE) functional[55] is used in calculations. The ion core potentials (nuclei and core electrons) are described with optimized norm-conserving Vanderbilt pseudopotentials with scalar-relativistic effects, provided by the Pseudo Dojo project.[56] Semicore 4s and 4p electrons of Ru are explicitly treated as valence electrons. Because Ru has moderate spin−orbit effects, we also did calculations for unipolar doping cases using VASP[57−59] with full relativistic effects and our main conclusions have not changed (as shown in Supporting Information).

Following previous works,[32,35] an effective Hubbard $U_{eff} = U - J = 2.0$ eV is used. We notice the Hubbard U_{eff} used in previous work ranges from 1.5 to 3.0 eV.[30,60] An experimental study suggests that $U = 2.4$ eV and $J = 0.4$ eV are reasonable guesses.[61] The dependence of our results on U_{eff} is studied and presented in Supporting Information.

The k-point grids of 6 × 3 × 1 and 15 × 8 × 1 are used for the Brillouin-zone sampling in intrinsic and doped cases, respectively. We set the distance d between neighboring layers as 15 Å to avoid spurious interactions. For structural optimizations, we relax both the atomic coordinates and the lattice constants so that residue forces are less than 2×10^{-4} Ry/a.u., stress are less than 0.05 kbar, and total energies are converged within 1×10^{-4} Ry. Because of the strong magnetic frustration,[29] there are many competing magnetic phases of monolayer $RuCl_3$. Even though these local minima phases may have the same total magnetization, the local distributions of spin polarization can be different and result in slightly different relaxed structures and total energies. We have performed structural relaxations with different starting points to find the structure with the lowest energy.

We constructed maximally localized wannier functions (MLWF) for the Cl p-orbitals and Ru t_{2g} orbitals using the Wannier90 package.[62,63] The hopping integrals between Ru t_{2g} orbitals is obtained from the tight-binding Hamiltonian built with MLWF.

We point out that the first-principles simulations of correlated magnetic materials, in particular for the highly frustrated system like $RuCl_3$, can be affected by the choice of functionals, pseudopotentials, effective Hubbard term U_{eff} and spin−orbit coupling (SOC). In Supporting Information, we discussed their impacts and find that these factors can affect our results quantitatively. For example, the relative energies calculated by different exchange-correlation functionals can differ by 6 meV/f.u. Nevertheless, our main conclusions that is, the enhancement of ferromagnetism under doping conditions, still hold (see Supporting Information Section 1).

We extract the exchange coupling constants up to the third-nearest neighbor by mapping the total energies of monolayer

DOI: 10.1021/acs.nanolett.9b02523
Nano Lett. 2019, 19, 7673−7680

$RuCl_3$ of four different magnetic orders to the Ising model on 2D hexagonal lattices

$$H = -\frac{1}{2}\left(\sum_{\langle i,j\rangle} J_1 S_i S_j + \sum_{\langle\langle i,j\rangle\rangle} J_2 S_i S_j + \sum_{\langle\langle\langle i,j\rangle\rangle\rangle} J_3 S_i S_j\right) \quad (1)$$

where $S_{1,2} = \pm 1/2$ and J_1, J_2, and J_3 correspond to exchange coupling constants between the NN, second NN, and third NN couplings.

With the Ising model, the exchange energies for four magnetic phases are given by

$$E_{\mathrm{FM}} = \frac{1}{4}(-6J_1 - 12J_2 - 6J_3) \quad (2)$$

$$E_{zz\mathrm{AFM}} = \frac{1}{4}(-2J_1 + 4J_2 + 6J_3) \quad (3)$$

$$E_{\mathrm{Neel}} = \frac{1}{4}(6J_1 - 12J_2 + 6J_3) \quad (4)$$

$$E_{\mathrm{stripy}} = \frac{1}{4}(2J_1 + 4J_2 - 6J_3) \quad (5)$$

For the MC simulation, we employ a hexagonal lattice with 60×60 spin sites, which is large enough to eliminate finite-size effects. To converge the canonical ensemble average magnetization, we ran the simulation with 1.3×10^5 Monte Carlo steps for each temperature points. We provide results of MC simulations for several doping densities in Supporting Information.

■ ASSOCIATED CONTENT

Supporting Information

Supporting Information include . The Supporting Information is available free of charge on the ACS Publications website at DOI: 10.1021/acs.nanolett.9b02523.

Tests on results with a range of U_{eff}, spin−orbit coupling effects, other exchange-correlation functionals; details on projected density of states for Ru t_{2g} orbitals, calculation of hopping integrals, and Monte Carlo simulations (PDF)

■ AUTHOR INFORMATION

Corresponding Authors

*(J.R.C.) E-mail: jrc@utexas.edu. Phone: 512-471-3312.

*(L.Y.) E-mail: lyang@physics.wustl.edu. Phone: 314-935-9453.

ORCID

Weiwei Gao: 0000-0003-4477-393X

Erik A. Henriksen: 0000-0002-4978-2440

James R. Chelikowsky: 0000-0003-2181-3070

Li Yang: 0000-0002-8611-6359

Author Contributions

⊥Y.T. and W.G. contributed equally to this work.

Notes

The authors declare no competing financial interest.

■ ACKNOWLEDGMENTS

L.Y. and E.A.H. acknowledge financial support from Washington University in St. Louis and the Institute of Materials Science and Engineering for the use of instruments and staff assistance. We thank Dr. Yan Lyu and Dr. Ruixiang Fei for their helpful discussions. Y.T. and L.Y. are supported by the National Science Foundation (NSF) CAREER Grant DMR-1455346 and the Air Force Office of Scientific Research (AFOSR) Grant FA9550-17-1-0304. E.A.H. acknowledges support under NSF DMR-1810305. Work at the University of Texas at Austin was supported from a subaward from the Center for Computational Study of Excited-State Phenomena in Energy Materials at the Lawrence Berkeley National Laboratory, which is funded by the U.S. Department of Energy, Office of Science, Basic Energy Sciences, Materials Sciences and Engineering Division under Contract No. DEAC0205CH11231, as part of the Computational Materials Sciences Program. Computational resources are provided by the Texas Advanced Computing Center (TACC).

■ REFERENCES

(1) Ma, Y.; Dai, Y.; Guo, M.; Niu, C.; Zhu, Y.; Huang, B. Evidence of the Existence of Magnetism in Pristine VX_2 Monolayers (X = S, Se) and Their Strain-Induced Tunable Magnetic Properties. *ACS Nano* **2012**, *6*, 1695−1701.

(2) Zhou, Y.; Wang, Z.; Yang, P.; Zu, X.; Yang, L.; Sun, X.; Gao, F. Tensile Strain Switched Ferromagnetism in Layered NbS_2 and $NbSe_2$. *ACS Nano* **2012**, *6*, 9727−9736.

(3) Yazyev, O. V. Emergence of magnetism in graphene materials and nanostructures. *Rep. Prog. Phys.* **2010**, *73*, 056501.

(4) Han, W.; Kawakami, R. K.; Gmitra, M.; Fabian, J. Graphene spintronics. *Nat. Nanotechnol.* **2014**, *9*, 794−807.

(5) Haugen, H.; Huertas-Hernando, D.; Brataas, A. Spin transport in proximity-induced ferromagnetic graphene. *Phys. Rev. B: Condens. Matter Mater. Phys.* **2008**, *77*, 115406.

(6) Huang, B.; Clark, G.; Navarro-Moratalla, E.; Klein, D. R.; Cheng, R.; Seyler, K. L.; Zhong, D.; Schmidgall, E.; McGuire, M. A.; Cobden, D. H.; Yao, W.; Xiao, D.; Jarillo-Herrero, P.; Xu, X. Layer-dependent ferromagnetism in a van der Waals crystal down to the monolayer limit. *Nature* **2017**, *546*, 270−273.

(7) Gong, C.; Li, L.; Li, Z.; Ji, H.; Stern, A.; Xia, Y.; Cao, T.; Bao, W.; Wang, C.; Wang, Y.; Qiu, Z. Q.; Cava, R. J.; Louie, S. G.; Xia, J.; Zhang, X. Discovery of intrinsic ferromagnetism in two-dimensional van der Waals crystals. *Nature* **2017**, *546*, 265−269.

(8) Lin, M.-W.; Zhuang, H. L.; Yan, J.; Ward, T. Z.; Puretzky, A. A.; Rouleau, C. M.; Gai, Z.; Liang, L.; Meunier, V.; Sumpter, B. G.; Ganesh, P.; Kent, P. R. C.; Geohegan, D. B.; Mandrus, D. G.; Xiao, K. Ultrathin nanosheets of $CrSiTe_3$: a semiconducting two-dimensional ferromagnetic material. *J. Mater. Chem. C* **2016**, *4*, 315−322.

(9) Bonilla, M.; Kolekar, S.; Ma, Y.; Diaz, H. C.; Kalappattil, V.; Das, R.; Eggers, T.; Gutierrez, H. R.; Phan, M.-H.; Batzill, M. Strong room-temperature ferromagnetism in VSe_2 monolayers on van der Waals substrates. *Nat. Nanotechnol.* **2018**, *13*, 289−293.

(10) Deng, Y.; Yu, Y.; Song, Y.; Zhang, J.; Wang, N. Z.; Sun, Z.; Yi, Y.; Wu, Y. Z.; Wu, S.; Zhu, J.; Wang, J.; Chen, X. H.; Zhang, Y. Gate-tunable room-temperature ferromagnetism in two-dimensional Fe_3GeTe_2. *Nature* **2018**, *563*, 94−99.

(11) O'Hara, D. J.; Zhu, T.; Trout, A. H.; Ahmed, A. S.; Luo, Y. K.; Lee, C. H.; Brenner, M. R.; Rajan, S.; Gupta, J. A.; McComb, D. W.; Kawakami, R. K. Room Temperature Intrinsic Ferromagnetism in Epitaxial Manganese Selenide Films in the Monolayer Limit. *Nano Lett.* **2018**, *18*, 3125−3131.

(12) Gong, C.; Zhang, X. Two-dimensional magnetic crystals and emergent heterostructure devices. *Science* **2019**, *363*, eaav4450.

(13) Jiang, S.; Li, L.; Wang, Z.; Shan, J.; Mak, K. F. Spin tunnel field-effect transistors based on two-dimensional van der Waals heterostructures. *Nat. Electron.* **2019**, *2* (4), 159−163.

(14) Huang, B.; Clark, G.; Klein, D. R.; MacNeill, D.; Navarro-Moratalla, E.; Seyler, K. L.; Wilson, N.; McGuire, M. A.; Cobden, D. H.; Xiao, D.; Yao, W.; Jarillo-Herrero, P.; Xu, X. Electrical control of 2D magnetism in bilayer CrI_3. *Nat. Nanotechnol.* **2018**, *13*, 544−548.

DOI: 10.1021/acs.nanolett.9b02523
Nano Lett. 2019, 19, 7673−7680

(15) Jiang, S.; Li, L.; Wang, Z.; Mak, K. F.; Shan, J. Controlling magnetism in 2D CrI_3 by electrostatic doping. *Nat. Nanotechnol.* **2018**, *13*, 549−553.
(16) Britnell, L.; Ribeiro, R. M.; Eckmann, A.; Jalil, R.; Belle, B. D.; Mishchenko, A.; Kim, Y.-J.; Gorbachev, R. V.; Georgiou, T.; Morozov, S. V.; Grigorenko, A. N.; Geim, A. K.; Casiraghi, C.; Neto, A. H. C.; Novoselov, K. S. Strong Light-Matter Interactions in Heterostructures of Atomically Thin Films. *Science* **2013**, *340*, 1311−1314.
(17) Bernardi, M.; Palummo, M.; Grossman, J. C. Extraordinary Sunlight Absorption and One Nanometer Thick Photovoltaics Using Two-Dimensional Monolayer Materials. *Nano Lett.* **2013**, *13*, 3664−3670.
(18) Guo, Y.; Sun, D.; Ouyang, B.; Raja, A.; Song, J.; Heinz, T. F.; Brus, L. E. *Nano Lett.* **2015**, *15* (8), 5081−5088.
(19) Lysenko, S.; Rua, A. J.; Vikhnin, V.; Jimenez, J.; Fernandez, F.; Liu, H. Light-induced ultrafast phase transitions in VO2 thin film. *Appl. Surf. Sci.* **2006**, *252*, 5512−5515.
(20) Hilton, D. J.; Prasankumar, R. P.; Fourmaux, S.; Cavalleri, A.; Brassard, D.; El Khakani, M. A.; Kieffer, J. C.; Taylor, A. J.; Averitt, R. D. Enhanced Photosusceptibility near T_c for the Light-Induced Insulator-to-Metal Phase Transition in Vanadium Dioxide. *Phys. Rev. Lett.* **2007**, *99*, 226401.
(21) Yuan, X.; Zhang, W.; Zhang, P. Hole-lattice coupling and photoinduced insulator-metal transition in VO_2. *Phys. Rev. B: Condens. Matter Mater. Phys.* **2013**, *88*, 035119.
(22) Náfrádi, B.; Szirmai, P.; Spina, M.; Lee, H.; Yazyev, O. V.; Arakcheeva, A.; Chernyshov, D.; Gibert, M.; Forró, L.; Horváth, E. Optically switched magnetism in photovoltaic perovskite CH3NH3-(Mn:Pb)I3. *Nat. Commun.* **2016**, *7*, 13406.
(23) Kimel, A. V.; Kirilyuk, A.; Tsvetkov, A.; Pisarev, R. V.; Rasing, T. Laser-induced ultrafast spin reorientation in the antiferromagnet $TmFeO_3$. *Nature* **2004**, *429* (6994), 850−853.
(24) Vahaplar, K.; Kalashnikova, A. M.; Kimel, A. V.; Hinzke, D.; Nowak, U.; Chantrell, R.; Tsukamoto, A.; Itoh, A.; Kirilyuk, A.; Rasing, T. Ultrafast Path for Optical Magnetization Reversal via a Strongly Nonequilibrium State. *Phys. Rev. Lett.* **2009**, *103* (11), 117201.
(25) Fausti, D.; Tobey, R. I.; Dean, N.; Kaiser, S.; Dienst, A.; Hoffmann, M. C.; Pyon, S.; Takayama, T.; Takagi, H.; Cavalleri, A. Light-Induced Superconductivity in a Stripe-Ordered Cuprate. *Science* **2011**, *331*, 189−191.
(26) Haleoot, R.; Paillard, C.; Kaloni, T. P.; Mehboudi, M.; Xu, B.; Bellaiche, L.; Barraza-Lopez, S. Photostrictive Two-Dimensional Materials in the Monochalcogenide Family. *Phys. Rev. Lett.* **2017**, *118*, 227401.
(27) Zhou, B.; Wang, Y.; Osterhoudt, G. B.; Lampen-Kelley, P.; Mandrus, D.; He, R.; Burch, K. S.; Henriksen, E. A. Possible structural transformation and enhanced magnetic fluctuations in exfoliated α-$RuCl_3$. *J. Phys. Chem. Solids* **2019**, *128*, 291.
(28) Mashhadi, S.; Weber, D.; Schoop, L. M.; Schulz, A.; Lotsch, B. V.; Burghard, M.; Kern, K. Electrical Transport Signature of the Magnetic Fluctuation-Structure Relation in α-$RuCl_3$ Nanoflakes. *Nano Lett.* **2018**, *18*, 3203−3208.
(29) Du, L.; Huang, Y.; Wang, Y.; Wang, Q.; Yang, R.; Tang, J.; Liao, M.; Shi, D.; Shi, Y.; Zhou, X.; Zhang, Q.; Zhang, G. 2D proximate quantum spin liquid state in atomic-thin α-$RuCl_3$. *2D Mater.* **2019**, *6* (1), 015014.
(30) Johnson, R. D.; Williams, S. C.; Haghighirad, A. A.; Singleton, J.; Zapf, V.; Manuel, P.; Mazin, I. I.; Li, Y.; Jeschke, H. O.; Valentí, R.; Coldea, R. Monoclinic crystal structure of α−$RuCl_3$ and the zigzag antiferromagnetic ground state. *Phys. Rev. B: Condens. Matter Mater. Phys.* **2015**, *92*, 235119.
(31) Sandilands, L. J.; Tian, Y.; Plumb, K. W.; Kim, Y.-J.; Burch, K. S. Scattering Continuum and Possible Fractionalized Excitations in α−$RuCl_3$. *Phys. Rev. Lett.* **2015**, *114*, 147201.
(32) Kim, H.-S.; Kee, H.-Y. Crystal structure and magnetism in α−$RuCl_3$: An ab initio study. *Phys. Rev. B: Condens. Matter Mater. Phys.* **2016**, *93*, 155143.
(33) Mermin, N. D.; Wagner, H. Absence of Ferromagnetism or Antiferromagnetism in One- or Two-Dimensional Isotropic Heisenberg Models. *Phys. Rev. Lett.* **1966**, *17*, 1133−1136.
(34) Rau, J. G.; Lee, E. K.-H.; Kee, H.-Y. Generic Spin Model for the Honeycomb Iridates beyond the Kitaev Limit. *Phys. Rev. Lett.* **2014**, *112*, 077204.
(35) Iyikanat, F.; Yagmurcukardes, M.; Senger, R. T.; Sahin, H. Tuning electronic and magnetic properties of monolayer α-$RuCl_3$ by in-plane strain. *J. Mater. Chem. C* **2018**, *6*, 2019−2025.
(36) Momma, K.; Izumi, F. VESTA 3 for three-dimensional visualization of crystal, volumetric and morphology data. *J. Appl. Crystallogr.* **2011**, *44* (6), 1272−1276.
(37) Sarikurt, S.; Kadioglu, Y.; Ersan, F.; Vatansever, E.; Aktürk, O. Ü.; Yüksel, Y.; Akıncı, Ü.; Aktürk, E. Electronic and magnetic properties of monolayer α-$RuCl_3$: a first-principles and Monte Carlo study. *Phys. Chem. Chem. Phys.* **2018**, *20* (2), 997−1004.
(38) Cao, T.; Li, Z.; Louie, S. G. Tunable Magnetism and Half-Metallicity in Hole-Doped Monolayer GaSe. *Phys. Rev. Lett.* **2015**, *114*, 236602.
(39) Li, X.; Wu, X.; Yang, J. Half-Metallicity in $MnPSe_3$ Exfoliated Nanosheet with Carrier Doping. *J. Am. Chem. Soc.* **2014**, *136*, 11065−11069.
(40) Liu, J.; Sun, Q.; Kawazoe, Y.; Jena, P. Exfoliating biocompatible ferromagnetic Cr-trihalide monolayers. *Phys. Chem. Chem. Phys.* **2016**, *18*, 8777−8784.
(41) Cococcioni, M.; de Gironcoli, S. Linear response approach to the calculation of the effective interaction parameters in the LDA+U method. *Phys. Rev. B: Condens. Matter Mater. Phys.* **2005**, *71*, 035105.
(42) Tiberj, A.; Rubio-Roy, M.; Paillet, M.; Huntzinger, J.-R.; Landois, P.; Mikolasek, M.; Contreras, S.; Sauvajol, J.-L.; Dujardin, E.; Zahab, A.-A. Reversible optical doping of graphene. *Sci. Rep.* **2013**, *3*, 2355.
(43) Han, T.-R. T.; Zhou, F.; Malliakas, C. D.; Duxbury, P. M.; Mahanti, S. D.; Kanatzidis, M. G.; Ruan, C.-Y. Exploration of metastability and hidden phases in correlated electron crystals visualized by femtosecond optical doping and electron crystallography. *Sci. Adv.* **2015**, *1*, e1400173.
(44) Chernikov, A.; Ruppert, C.; Hill, H. M.; Rigosi, A. F.; Heinz, T. F. Population inversion and giant bandgap renormalization in atomically thin WS_2 layers. *Nat. Photonics* **2015**, *9*, 466−470.
(45) Abtew, T. A.; Sun, Y. Y.; Shih, B.-C.; Dev, P.; Zhang, S. B.; Zhang, P. Dynamic Jahn-Teller Effect in the NV^- Center in Diamond. *Phys. Rev. Lett.* **2011**, *107* (14), 146403.
(46) Dreyer, C. E.; Alkauskas, A.; Lyons, J. L.; Janotti, A.; Van de Walle, C. G. First-Principles Calculations of Point Defects for Quantum Technologies. *Annu. Rev. Mater. Res.* **2018**, *48* (1), 1−26.
(47) Paillard, C.; Xu, B.; Dkhil, B.; Geneste, G.; Bellaiche, L. Photostriction in Ferroelectrics from Density Functional Theory. *Phys. Rev. Lett.* **2016**, *116* (24), 247401−247401.
(48) Wang, H.; Zhang, C.; Rana, F. Ultrafast Dynamics of Defect-Assisted Electron−Hole Recombination in Monolayer MoS_2. *Nano Lett.* **2015**, *15*, 339−345.
(49) Beaurepaire, E.; Merle, J. C.; Daunois, A.; Bigot, J. Y. Ultrafast Spin Dynamics in Ferromagnetic Nickel. *Phys. Rev. Lett.* **1996**, *76* (22), 4250−4253.
(50) Zhang, G. P.; Hübner, W.; Lefkidis, G.; Bai, Y.; George, T. F. Paradigm of the time-resolved magneto-optical Kerr effect for femtosecond magnetism. *Nat. Phys.* **2009**, *5*, 499.
(51) Marzari, N.; Mostofi, A. A.; Yates, J. R.; Souza, I.; Vanderbilt, D. Maximally localized Wannier functions: Theory and applications. *Rev. Mod. Phys.* **2012**, *84* (4), 1419−1475.
(52) Plumb, K. W.; Clancy, J. P.; Sandilands, L. J.; Shankar, V. V.; Hu, Y. F.; Burch, K. S.; Kee, H.-Y.; Kim, Y.-J. $RuCl_3$: A spin-orbit assisted Mott insulator on a honeycomb lattice. *Phys. Rev. B: Condens. Matter Mater. Phys.* **2014**, *90* (4), 041112.
(53) Giannozzi, P.; Baroni, S.; Bonini, N.; Calandra, M.; Car, R.; Cavazzoni, C.; Ceresoli, D.; Chiarotti, G. L.; Cococcioni, M.; Dabo, I.; Dal Corso, A.; de Gironcoli, S.; Fabris, S.; Fratesi, G.; Gebauer, R.; Gerstmann, U.; Gougoussis, C.; Kokalj, A.; Lazzeri, M.; Martin-

DOI: 10.1021/acs.nanolett.9b02523
Nano Lett. 2019, 19, 7673−7680

Samos, L.; Marzari, N.; Mauri, F.; Mazzarello, R.; Paolini, S.; Pasquarello, A.; Paulatto, L.; Sbraccia, C.; Scandolo, S.; Sclauzero, G.; Seitsonen, A. P.; Smogunov, A.; Umari, P.; Wentzcovitch, R. M. QUANTUM ESPRESSO: a modular and open-source software project for quantum simulations of materials. *J. Phys.: Condens. Matter* **2009**, *21*, 395502.

(54) Giannozzi, P.; Andreussi, O.; Brumme, T.; Bunau, O.; Buongiorno Nardelli, M.; Calandra, M.; Car, R.; Cavazzoni, C.; Ceresoli, D.; Cococcioni, M.; Colonna, N.; Carnimeo, I.; Dal Corso, A.; de Gironcoli, S.; Delugas, P.; DiStasio, R. A.; Ferretti, A.; Floris, A.; Fratesi, G.; Fugallo, G.; Gebauer, R.; Gerstmann, U.; Giustino, F.; Gorni, T.; Jia, J.; Kawamura, M.; Ko, H.-Y.; Kokalj, A.; Küçükbenli, E.; Lazzeri, M.; Marsili, M.; Marzari, N.; Mauri, F.; Nguyen, N. L.; Nguyen, H.-V.; Otero-de-la-Roza, A.; Paulatto, L.; Poncé, S.; Rocca, D.; Sabatini, R.; Santra, B.; Schlipf, M.; Seitsonen, A. P.; Smogunov, A.; Timrov, I.; Thonhauser, T.; Umari, P.; Vast, N.; Wu, X.; Baroni, S. Advanced capabilities for materials modelling with Quantum ESPRESSO. *J. Phys.: Condens. Matter* **2017**, *29*, 465901.

(55) Perdew, J. P.; Burke, K.; Ernzerhof, M. Generalized Gradient Approximation Made Simple. *Phys. Rev. Lett.* **1996**, *77* (18), 3865−3868.

(56) van Setten, M. J.; Giantomassi, M.; Bousquet, E.; Verstraete, M. J.; Hamann, D. R.; Gonze, X.; Rignanese, G.-M. The PseudoDojo: Training and grading a 85 element optimized norm-conserving pseudopotential table. *Comput. Phys. Commun.* **2018**, *226*, 39−54.

(57) Kresse, G.; Furthmüller, J. Efficiency of ab-initio total energy calculations for metals and semiconductors using a plane-wave basis set. *Comput. Mater. Sci.* **1996**, *6* (1), 15−50.

(58) Kresse, G.; Furthmüller, J. Efficient iterative schemes for ab initio total-energy calculations using a plane-wave basis set. *Phys. Rev. B: Condens. Matter Mater. Phys.* **1996**, *54* (16), 11169−11186.

(59) Kresse, G.; Joubert, D. From ultrasoft pseudopotentials to the projector augmented-wave method. *Phys. Rev. B: Condens. Matter Mater. Phys.* **1999**, *59* (3), 1758−1775.

(60) Kim, H.-S.; V, V. S.; Catuneanu, A.; Kee, H.-Y. Kitaev magnetism in honeycomb $RuCl_3$ with intermediate spin-orbit coupling. *Phys. Rev. B: Condens. Matter Mater. Phys.* **2015**, *91*, 241110.

(61) Sandilands, L. J.; Tian, Y.; Reijnders, A. A.; Kim, H.-S.; Plumb, K. W.; Kim, Y.-J.; Kee, H.-Y.; Burch, K. S. Spin-orbit excitations and electronic structure of the putative Kitaev magnet $RuCl_3$. *Phys. Rev. B: Condens. Matter Mater. Phys.* **2016**, *93* (7), 075144.

(62) Mostofi, A. A.; Yates, J. R.; Lee, Y.-S.; Souza, I.; Vanderbilt, D.; Marzari, N. wannier90: A tool for obtaining maximally-localised Wannier functions. *Comput. Phys. Commun.* **2008**, *178* (9), 685−699.

(63) Mostofi, A. A.; Yates, J. R.; Pizzi, G.; Lee, Y.-S.; Souza, I.; Vanderbilt, D.; Marzari, N. An updated version of wannier90: A tool for obtaining maximally-localised Wannier functions. *Comput. Phys. Commun.* **2014**, *185* (8), 2309−2310.

DOI: 10.1021/acs.nanolett.9b02523
Nano Lett. 2019, 19, 7673−7680